Mutational Analysis of the K^+-Competitive Inhibitor Site of Gastric H,K-ATPase†

Olga Vagin,‡ Keith Munson,‡ Nils Lambrecht,§ Steven J. D. Karlish,|| and George Sachs*,‡

Department of Physiology and Medicine, UCLA and VAGLAHS, and Department of Pathology, UCLA, Los Angeles, California 90073, and Department of Biological Chemistry, Weizmann Institute of Science, Rehovot, 76100, Israel

Received March 15, 2001; Revised Manuscript Received May 7, 2001

ABSTRACT: The gastric H,K-ATPase is inhibited selectively and K^+-competitively from its luminal surface by protonated imidazo[1,2α]pyridines (e.g., SCH28080). Identification of the amino acids in the membrane domain that affect SCH28080 inhibition should provide a template for modeling a luminally directed vestibule in this enzyme, based on the crystal structure of the sr Ca-ATPase. Five conserved carboxylic residues, Glu343, Glu795, Glu820, Asp824, Glu936, and unique Lys791 in the H,K-ATPase were mutated, and the effects of mutations on the K_i for SCH28080, V_{max}, and $K_{m,app}[NH_4^+]$ were measured. A kinetic analysis of the ATP hydrolysis data indicated that all of these residues significantly affect the interaction of NH_4^+ ions with the protein but only three of them, Glu795, Glu936, and Lys791, greatly affected SCH28080 inhibition. A Glu795Asp mutation increased the K_i from 64 ± 11 to 700 ± 110 nM. Since, however, the mutation Glu795Gln did not change the K_i (86 ± 31 nM), this site has a significant spatial effect on inhibitor kinetics. A Glu936Asp mutation resulted in noncompetitive kinetics while Gln substitution had no effect either on inhibitor affinity or on the nature of the kinetics, suggesting that the length of the Glu936 side chain is critical for the exclusive binding of the ion and SCH28080. Mutation of Lys791 to Ser, the residue present in the SCH28080-insensitive Na,K-ATPase, resulted in a 20-fold decrease in SCH28080 affinity, suggesting an important role of this residue in SCH28080 selectivity of the H,K-ATPase versus Na,K-ATPase. Mutations of Asp824, Glu343, and Glu820 increased the K_i 2−3-fold, implying a relatively minor role for these residues in SCH28080 inhibition. It appears that the imidazopyridine moiety of SCH28080 in the protonated state interacts with residues near the negatively charged residues of the empty ion site from the luminal side (TM4, -5, -6, and -8) while the hydrophobic phenyl ring interacts with TM1 or TM2 (the latter conclusion based on previous data from photoaffinity labeling). The integrity of the SCH28080 binding site depends on the presence of Lys791, Glu936, and Glu795 in H,K-ATPase. A computer-generated model of this region illustrates the possible involvement of the residues previously shown to affect SCH28080 inhibition (Cys813, Ile816, Thr823, Met334, Val337) and may predict other residues that line the SCH28080 binding vestibule in the E_2 conformation of the pump.

The gastric H,K-ATPase (HK α1) is responsible for generating gastric acid by pumping protons or hydronium ions out of the parietal cell of the stomach in exchange for potassium. The enzyme has 10 transmembrane helices (TM)[1] in the catalytic α subunit, like other P_2-type ATPases, and a single TM in the accessory β subunit (*1*−*6*), like the Na,K-ATPase. Both are K^+ counter-transport pumps with 75% homology between their catalytic subunits, but differing markedly in their inhibitor sensitivity. Ouabain inhibits the Na,K-ATPase but not the H,K-ATPase, and, conversely, the smaller imidazo[1,2α]pyridine, SCH28080, inhibits the H,K-ATPase but not the Na,K-ATPase. Both inhibitors gain access to their binding sites from the extracytoplasmic surface. SCH28080 is strictly K^+-competitive and is active in its protonated form. Knowledge of the amino acids that affect inhibition by SCH28080 should provide insight into the regions of the membrane domain of the H,K-ATPase that are responsible for the exclusive interaction of K^+ and SCH28080 and for the selectivity of SCH28080 for this ion pump.

The large size of the protonated imidazopyridine compared to K^+ (or its surrogate NH_4^+) suggests that the sets of amino acid residues forming ion and inhibitor binding sites are not identical and there must be residues binding SCH28080 that do not bind K^+ and vice versa. For example, mutations of several residues in the membrane domain have been shown to reduce the affinity for SCH28080, namely, Cys813 in TM5 (*7*), Ile816 and Pro827 in TM6 (*8*), and Met334 and Val337 in TM4 (*9*), without a significant effect on ion affinity. These residues likely contribute to SCH28080 binding and not K^+ binding.

† Supported in part by NIH Grants DK46917, 53462, 41301, and 17294.

* Correspondenc should be addressed to this author at VAGLAHS/West LA, Building 113, Room 326, 11301 Wilshire Blvd., Los Angeles, CA 90073. Phone: 310-268-4672. Fax: 310-312-9478. E-mail: gsachs@ucla.edu.

‡ UCLA and VAGLAHS.

§ UCLA.

|| Weizmann Institute of Science.

[1] Abbreviations: G1, hog gastric vesicles; K_i[SCH28080], apparent affinity for inhibitor; $K_{m,app}[NH_4^+]$, apparent affinity for cation (NH_4^+); P_i, inorganic phosphate; PIPES, piperazine-*N*,*N*′-bis(2-ethanesulfonic acid); SCH28080, 3-cyanomethyl-2-methyl-8-(phenylmethoxy)imidazo-[1,2α]pyridine; sr Ca-ATPase, sarcoplasmic reticulum Ca-ATPase; TM, transmembrane helix; V_{max}, maximal specific activity; wt, wild type.

10.1021/bi0105328 CCC: $20.00
Published on Web 06/02/2001

However, the purely competitive nature of SCH28080 inhibition with respect to stimulating counterion (K^+ or NH_4^+) suggests that some of the ion binding residues are also involved in inhibitor binding. The side chains involved in cation binding reside near the middle of the membrane domain in the P_2-type ATPases. Carboxylic and oxygen-containing acid side chains in TM4, -5, -6, and -8 homologous to the Glu343, Glu795, Glu820, Thr823, Asp824, and Glu936 of H,K-ATPase have been shown to be involved in ion binding in Ca-ATPase and Na,K-ATPase based on results of site-directed mutagenesis (*10*−*16*) which are consistent with the Ca^{2+}-containing crystal structure of the E_1 form of the sr Ca-ATPase at 2.6 Å (*17*). Other oxygen-containing amino acids are also candidates for ion-coordinating residues. For example, the mutation Ser775Ala in the Na,K-ATPase (which corresponds to Lys791 in H,K-ATPase) resulted in a 30-fold decrease in K^+ affinity (*18*). The inhibition kinetics of SCH28080 have been defined thus far with mutation of only two of the putative ion binding residues, namely, Glu820 (*19, 20*) and Thr823 (*8*).

Understanding binding requirements and improving inhibitor design clearly require a model of the molecular structure of the H,K-ATPase. Since three-dimensional crystallization of the H,K-ATPase has not yet been possible, a model for the membrane domain of the catalytic subunit was constructed by placing the H,K-ATPase side chains on homologous α-carbon positions of the known 3D structure of the sr Ca-ATPase. It has been shown that the yeast proton pump and the sr Ca-ATPase, each examined at 8 Å resolution, have closely overlapping density envelopes in the membrane domain even though crystallized in different conformations, E_1 and E_2, respectively. Moreover, the same yeast pump E_1 structure, obtained by electron diffraction, closely overlaps the higher resolution structure of the E_1 form of sr Ca-ATPase derived from X-ray diffraction (*21*). Therefore, the 35% sequence homology between these two distantly related P_2-type ATPases underlies a more fundamental structural homology as typically found in families of soluble proteins. This provides an experimental basis for homology modeling of the H,K-ATPase membrane domain with that of the high-resolution structure of the sr Ca-ATPase.

In the present study, we report the effect of conservative and nonconservative mutations of Glu343, Glu795, Glu820, Asp824, Glu936, and Lys791 on ion and SCH28080 affinity and provide a model illustrating the possible involvement of these residues in SCH28080 inhibition.

MATERIALS AND METHODS

Vectors Used for the Expression of the H,K-ATPase α and β Subunits. The cDNA coding for the rabbit H,K-ATPase α subunit (*22*) (GenBank accession number X64694) was inserted into the multiple cloning site of the mammalian expression vector pcDNA3.1(Zeo) (Invitrogen, Carlsbad, CA) containing the eukaryotic selection marker Zeocin (Invitrogen) to form pcDNA3.1(Zeo)-H,K-α. The cDNA coding for the rabbit H,K-ATPase β subunit (*23*) (GenBank accession number M35544) was inserted into the multiple cloning site of the mammalian expression vector pcDNA3-(G418) (Invitrogen) containing the eukaryotic selection marker G418 for neomycin resistance [pcDNA3(G418)-H,K-β].

Site-Directed Mutagenesis of Glu343, Glu795, Glu820, Asp824, Glu936, and Lys791. The mutations Glu343 to Gln, Ala, and Asp; Glu795 to Gln and Asp; Glu820 to Gln, Ala, and Asp; Asp824 to Asn, Ala, and Glu; Glu936 to Gln and Asp; and Lys291 to Ser were generated by using the Quickchange mutagenesis kit (Stratagene, La Jolla, CA). The plasmid pcDNA3.1(Zeo)-H,K-α was used as a template. Each final construct was sequenced before use in transfection.

Transfection of HEK293 Cells and Selection of Stable Cell Lines. Human embryonic kidney cells (HEK293-ATCC CRL 1573) were transfected with pcDNA3(G418)-H,K-β as previously reported (*24*), and a stable cell line was selected by adding at 60 h after transfection the eukaryotic selection marker G418 at a concentration of 0.75 mg of G418/mL of media. This concentration of G418 was maintained until single colonies appeared. The colonies were isolated, expanded, and grown in the presence of 0.25 mg of G418/mL of media. The stable expression of the H,K-ATPase β subunit was confirmed by Western blot analysis using a monoclonal antibody against the H,K-ATPase β subunit, as described below. The clone with the highest level of expression of the H,K-ATPase β subunit (*9*) was then subjected to a second transfection with pcDNA3.1(Zeo)-H,K-α containing either wt or mutant H,K-ATPase α subunit cDNAs. By adding the second eukaryotic selection marker Zeocin at a concentration of 0.4 mg/mL of media in addition to the maintenance concentration of G418 of 0.25 mg/mL of media, stable cell lines expressing H,K-ATPase α as well as β subunits were selected with good efficiency, as shown by Western blot analysis as described below. For each mutation, 15−20 cell lines were selected, and 2 clones with the best ratio of expressed H,K-ATPase to total protein were expanded for isolation of membranes. The maintenance concentration for Zeocin was 0.1 mg/mL of medium.

Preparation of Crude Membranes. Cell layers from stable cell lines were grown to confluence and left in the flasks for another 2−3 days until the cell culture became overgrown (cells grew on the top of the cells attached to the bottom of the flask) and the medium started to turn yellow. The medium was changed, and cells were left in the same flasks for 2 more days. The cells were resuspended in sodium-free buffer A [PIPES (10 mM)/EGTA (2 mM)/EDTA (2 mM), pH 7.0, containing 250 mM sucrose]. The cell suspension was homogenized with a tight Dounce homogenizer (Wheaton, Millwille, NY). The homogenate was collected, layered onto a 42% sucrose step gradient, and spun in a Beckman SW28 swinging-bucket rotor at 25 000 rpm for 1 h at 4 °C. The fraction at the interface of buffer/sucrose was collected and diluted to a total volume of 15 mL in buffer A. The membrane fraction was collected by centrifugation in a Beckman 75Ti rotor (35 000 rpm, 4 °C, 1 h). The pellet was resuspended in buffer A by homogenization with a 2 mL Teflon homogenizer (Wheaton). The total protein concentration was determined by the method of Bradford (*25*) with immunoglobulin G as a standard according to the manufacturer (BioRad Laboratories, Hercules, CA). The typical protein concentration was ≈10 μg/μL. The membranes were aliquoted, flash-frozen, and stored at −80 °C.

SDS−PAGE and Western Blot Analysis. Thirty microliters of gel sample buffer [4% SDS, 0.05% bromophenol blue (w/v), 20% glycerol, 1% β-mercaptoethanol (v/v) in 0.1 M Tris buffer, pH 6.8] containing membrane fraction (1−15

μg of protein) was loaded on a 7% SDS−polyacrylamide gel. As a standard for native α and β subunits, 40−170 ng of purified gastric vesicles (G1 fraction) (*26*) was used. Molecular weight standards (BioRad Laboratories) were loaded on each gel.

After SDS−PAGE, proteins were transferred to nitrocellulose membranes (BioPlot-NC, Costar, Cambridge, MA). Membranes were washed twice with TBS [10 mM Tris, 150 mM NaCl, 0.05% Tween (v/v)] and incubated in TBS containing 1% bovine serum albumin (w/v). After 30 min, the membranes were incubated in the primary antibody solution (monoclonal antibody 12.18 against amino acids 666−689 of the α subunit of the H,K-ATPase diluted 1:10 000 in TBS or monoclonal antibody 2B6 against amino acids 236−281 of the β subunit of the H,K-ATPase diluted 1:1000 in TBS). After 1 h, membranes were washed twice with TBS and incubated with the secondary antibody solution [anti-mouse IgG conjugated to alkaline phosphatase (Promega, Madison, WI), diluted 1:2000 in TBS]. Then, after 1 h, membranes were washed twice and incubated for 15 min in TBS. After a final wash, the membranes were incubated for 5 min in AP buffer (100 mM Tris, 100 mM NaCl, 5 mM $MgCl_2$, pH 9.5) containing 0.3% nitro blue tetrazolium solution (v/v) and 0.15% 5-bromo-4-chloro-3-indolyl-1-phosphate solution (v/v) according to the manufacturer's instructions (Promega).

Western blot analysis of the membranes isolated from the stably transfected cell lines indicated that all of them expressed the β subunit of various levels of glycosylation and the full-size α subunit (not shown).

Quantification of Expressed H,K-ATPase. The content of expressed H,K-ATPase in the membrane fraction was quantified by using purified hog gastric vesicles containing ≈85% H,K-ATPase (G1) (*26*) as a standard. Three different amounts of membrane fraction and three different amounts of G1 were loaded on the same gel. SDS−PAGE and Western blot analysis of the α subunit of the H,K-ATPase were done as described above. All blots were scanned using the AMBIS optical imaging system (AMBIS Inc., San Diego, CA), and the optical density of the bands was measured; 40−170 ng of purified G1 yielded a linear calibration curve. For each membrane preparation, the range of loaded amounts of membrane fraction giving similar values of the optical density as compared to the densities obtained for G1 was chosen. The amount of the α subunit of the H,K-ATPase in the sample was calculated using the calibration curve for G1. This allowed an estimate of the content of H,K-ATPase in crude membranes as the percent of total membrane protein. The level of expression for each membrane preparation was calculated as the average of values obtained for three amounts of loaded membrane fraction.

NH_4^+-Stimulated ATPase Activity. ATPase assays were performed by a modification of the method of Yoda and Hokin (*27*). One hundred and twenty-five microliters of Na^+-free reaction buffer [40 mM Tris-HCl (pH 7.4), 2 mM $MgCl_2$ with various ATPase inhibitors (1 mM EGTA (inhibition of Ca-ATPases), 500 μM ouabain (inhibition of Na,K-ATPase), 1 μM oligomycin (inhibition of mitochondrial ATPase), 10 nM bafilomycin (inhibition of V type ATPases), and 100 nM thapsigargin (inhibition of sr Ca-ATPase))] contained 1−3 μL of the membrane fraction, various concentrations of NH_4Cl (0−40 mM), and SCH28080 (0−2000 nM) as a selective inhibitor of the H,K-ATPase (*28*). The reaction was started by adding 25 μL of a 4.8 mM ATP solution with 10 000 cpm/nmol of [γ-^{32}P]ATP (ATP, 3000 Ci/mmol, Amersham Pharmacia Biotech, Piscataway, NJ). The reaction was terminated after 1 h at 37 °C by adding an equal volume of stop solution containing 4.5% ammonium molybdate (w/v) and 14% perchloric acid. The ammonium molybdate−P_i complex was extracted with 300 μL of butyl acetate, and the radioactivity was measured by scintillation counting. Ion-stimulated ATPase activity was calculated as a difference between P_i release in the presence and in the absence of NH_4Cl. The activity was expressed in micromoles of P_i per milligram of total protein per hour and then converted to specific H,K-ATPase activity (micromoles of P_i per milligram of H,K-ATPase per hour) relative to a purified gastric vesicle preparation (G1) using the values for H,K-ATPase content in the membranes obtained from the quantitative Western blot analysis (see above).

Determination of V_{max}, $K_{m,app}$ for NH_4^+, and K_i for SCH28080. Data for the specific H,K-ATPase activities at various NH_4Cl concentrations (15−24 points) in the absence of inhibitor or at fixed concentration of inhibitor were fitted by nonlinear regression to the Michaelis−Menten equation (Enzfitter, BIOSOFT, 1999), and the V_{max} ± SE and the apparent K_m ($K_{m,app}$) ± SE for NH_4^+ were obtained. Each set of data points was plotted as an inverse plot to determine the mechanism of SCH28080 inhibition (competitive, noncompetitive, or mixed). The K_i ± SE was obtained from linear regression of the $K_{m,app}/V_{max}$ values plotted vs inhibitor concentration. The intersection of the linear regression with *x*-axis gives the negative K_i.

H,K-ATPase Activity in the Absence of NH_4^+ (H-ATPase). Two micrograms of the membrane fraction in 125 μL of Na^+-free reaction buffer (the same as for NH_4^+-stimulated ATPase activity, see above) in the absence or in the presence of 10 μM SCH28080 was incubated with 25 μL of 15 μM ATP (final ATP 2.5 μM) containing 250 000 cpm/nmol [γ-^{32}P]ATP (ATP, 3000 Ci/mmol, Amersham Pharmacia Biotech) at 37 °C for 60 min. The reaction was terminated, and P_i release was determined as described above for NH_4^+-stimulated ATPase activity. The H-ATPase activity was determined as the difference between P_i release in the absence of SCH28080 and in the presence of SCH28080 and calculated as micromoles of P_i released for 1 h per milligram of H,K-ATPase using the values for H,K-ATPase content in the membranes obtained from the quantitative Western blot analysis (see above).

Computer Modeling. A homology-based model for the membrane domain of the gastric H,K-ATPase α subunit was constructed by using the 3D coordinates of the sr Ca-ATPase (pdb.1eul) as a starting framework (*17*). All model building and energy minimizations were performed with Discover and Insight II molecular modeling software by MSI Inc., San Diego, CA. The subdomains designated P, N, and A in the cytoplasmic domain of the sr Ca-ATPase are likely to be structurally homologous in all P_2-type ATPases, and these were not altered. The N and A subdomains are distant from the membrane and were fixed during energy minimizations.

Side chains from the H,K-ATPase sequence were mapped onto the equivalent positions in the membrane domain of the sr Ca-ATPase structure as identified by a combination of computer and manual sequence alignments. Where dif-

Table 1: Substitution of Residues of the sr Ca-ATPase by Residues of the H,K-ATPase in the Computer Model of the H,K-ATPase Membrane Domain Based on sr Ca-ATPase Crystal Structure

		TM1
HK:	**96**	G T **P E Y V K F A R Q L A G G L Q C L M W V A A A I C L I A F A I Q**
srCa:	**46**	G K **S L W E L V I E Q F E D L L V R I L L L A A C I S F V L A W F E**
		M1M2 loop
HK:	**130**	A S E G D L T T D D N L Y loop backbone from pdb2lhb: M88-N100
srCa:	**80**	E G E E T I - - - T A F V
		TM2
HK:	**143**	**L A L A L I A V V V V T G C F G Y Y Q E F K S**
srCa:	**90**	**E P F V I L L I L I A N A I V G V W Q E R N A**
		TM3
HK:	**292**	K **T P I A I E I E H F V D I I A G L A I L F G A T F F V**
srCa:	**246**	K **T P L Q Q K L D E F G E Q L S K V I S L I C V A V W L**
		M3M4 loop
HK:	**320**	**V A M C I G** - - - - - - - - - - **Y T F L R** loop backbone from pdb1opb: Y[A19]-T[A29]
srCa:	**274**	**I N** I G H F N D P V H G G S W I R G **A I Y**
		TM4
HK:	**331**	**A M V F F M A I V V A Y V P E G L L A T V T V C L**
srCa:	**295**	**Y F K I A V A L A V A A I P E G L P A V I T T C L**
		TM5 **M5M6 loop**
HK:	**779**	**I F D N L K K S I A Y T L T K N I P E L T P Y L I Y I T V** S V P L P L
srCa:	**753**	**I Y N N M K Q F I R Y L I S S N V G E V V C I F L T A A L** G L P E A L
		TM6 (continued from TM5) **M6M7 cytoplasmic loop**
HK:	**814**	**G C I T I L F I E L C T D I F P S V S L A Y** E K A E S D I M H L R P R N P K R D R L
srCa:	**788**	**I P V Q L L W V N L V T D G L P A T A L G F N** P P D L D I M D R P P R S P K E P L I
		TM7 (continued from TM6)
HK:	**856**	**V N E P L A A Y S Y F Q I G A I Q S F A G F** T D Y F T A M A Q E
srCa:	**830**	**S G W L F F R Y M A I G G Y V G A A T V G A** A A W W F M Y A E D
		TM8
HK:	**924**	**Y Q Q Y T C Y T V F F I S I E M C Q I A D V** L I R K
srCa:	**894**	**P E P M T M A L S V L V T I E M C N A L N S** L S E N
		M8M9 cytoplasmic loop
HK:	**950**	T R R L S A F Q Q G F F R N loop backbone from pdb1ova:L[C41]-P[C54]
srCa:	**920**	Q S L M R M P P - - - W V N
		TM9 (continued from TM8) **M9M10 loop**
HK:	**964**	**R I L V I A I V F Q V C I G C F L C Y C** P G M P N I F N F M P I
srCa:	**931**	**I W L L G S I C I S M S L H F L I L Y V** D P L P M I F K L K A L
		TM10 (continued from TM9)
HK:	**996**	**R F Q W W L V P M P F G L L I F V Y D E I R K L** G V
srCa:	**963**	**D L T Q W L M V L K I S L P V I G L D E I L K F** I A

ferences occurred in the number of residues between aligned membrane segments, the sr Ca-ATPase loops in the 3D structure were replaced by using the "search loop" command provided in the software. This subroutine searches a defined set of high-resolution database proteins for loops of designated size whose pre- and post-loop α-carbons closely overlap those of the target structure.

Matching segments from the rabbit gastric H,K-ATPase α sequence (HK, GenBank accession no. P27112) used for replacement of rabbit sr Ca-ATPase residues (GenBank sequence accession no. P04191) are given in Table 1 with boldface characters indicating regions of predicted α helix.

Some of the transmembrane segments in the H,K-ATPase contain prolines not found in the sr Ca-ATPase (two in TM5 and TM10 and one in TM7). Proline in helices either can not affect the helix or can alter the direction of the helix or expand the helical twist as in TM6 of the sr Ca-ATPase. In the absence of experimental data, the helical backbone as observed in the sr Ca-ATPase was not modified near the prolines in the present model. These proline substitutions could have structural consequences in the H,K-ATPase, especially in TM10 where two prolines occur within a three residue segment.

The Ca-ATPase residues from Gly[A862] to Ala[A893] (e.g., the M7M8 luminal loop) were left unaltered because the loop size and lack of sequence homology made modeling unfeasible. The region enclosing TM5, the M5M6 luminal loop, TM6, the M6M7 cytoplasmic loop, and TM7 has numerous functional amino acid homologies and an equivalent number of residues in H,K- and sr Ca-ATPases and was therefore replaced throughout. Similarly, TM9 through TM10 have the same number of residues, and no loop replacement was required.

The conformations of substituted side chains were assigned to mimic the volumes of the corresponding sr Ca-ATPase residues where possible. Overlapping side chain densities were resolved by assigning only those dihedrals found in known high-resolution helices. Then energy minimization (molecular mechanics) was performed using the consistent valence force field provided with the software to an average absolute derivative of approximately 0.1 kcal $(mol \cdot Å)^{-1}$. To improve the simulation in the vicinity of the ion binding residues, Lys791 was assigned a positive charge, Glu343, Glu820, and Asp824 were made negative, and Glu795 and Glu936 were kept neutral. These assignments were suggested by the results of various mutations described below. In

addition, hydronium ions were placed in the positions occupied by the two calcium ions in sr Ca-ATPase with hydrogen bonding to Glu343, Glu820, Asp824, and carbonyl oxygens of Val341 and Ala339 (site 1) and Asp824, Glu795, and Asn792 (site 2), respectively. In addition, four water molecules were placed in the space between apparent hydrogen bonding side chains Ser760 (TM5) and Ser 804 (TM6) (water 1), Thr788 (TM5) and the carbonyl oxygens of Glu343 and Gly344 (TM4) (water 2), Gln110 (M1) and Thr152 (M2) (water 3), and the carbonyl oxygens of Cys822 and Thr823 and the side chains of Thr 823, Lys791, Tyr787, and Gln971 (water 4). Energy minimization was then repeated to an average absolute derivative of 0.1 kcal $(mol\cdot Å)^{-1}$. After minimization, the positions of the membrane helices were only slightly changed in the H,K-ATPase model compared to the sr Ca-ATPase with an RMS deviation in the backbones of all the membrane helices (2296 atoms) of 1.15 Å. Finally, the effect of changing the first dihedral angle of Lys791 from its value in the original model (−60°) to the alternative orientation (180°) was examined. Energy minimization again to an average absolute derivative of 0.1 kcal $(mol\cdot Å)^{-1}$ displaced one hydronium from the ion binding site and gave hydrogen bonds between the protonated amino group and the side chain oxygens of Glu820, Asp824, and Asn792 with little change in the overall positions of the membrane helices (backbone RMS deviation over 2296 atoms of 0.360 Å).

To be consistent with the numbering in a large body of previous work including the original purification of the gastric H,K-ATPase, amino acid numbers used in this report will be those of the hog α subunit which is 98.5% identical to the rabbit. The hog sequence lacks one lysine residue near the amino terminus (position 31), and protein sequencing shows no N-terminal methionine. Therefore, position numbers for homologous residues given here are two less than the rabbit sequence.

RESULTS

K_i[SCH28080], V_{max}, and $K_{m,app}[NH_4^+]$ for the Expressed Wild-Type and Mutant H,K-ATPase. The basal activity of the membranes containing expressed wt H,K-ATPase, in the absence of added NH_4^+, was 1.1 μmol of P_i (mg of total protein)$^{-1}$ h^{-1}. Most of this background ATP hydrolysis is largely insensitive to SCH28080 and represents mainly the activity of unrelated ATPases. In the presence of 20 mM NH_4^+, the activity increased by about 4.5-fold (350% signal over background). The addition of 20 μM SCH28080 in the presence of 20 mM NH_4^+ inhibited the enzyme activity down to the basal level. Data points for the NH_4^+-activated ATP hydrolysis in the range of NH_4^+ concentrations (1−20 mM), in the absence of SCH28080, were fitted to the Michaelis−Menten equation and gave a $K_{m,app}[NH_4^+]$ of 2.4 ± 0.2 mM and a V_{max} of 182 ± 3.2 μmol (mg of H,K-ATPase)$^{-1}$ h^{-1} (Figure 1A, Table 2). Note that V_{max} is the maximum specific activity of the expressed enzyme (the velocity normalized to the amount of H,K-ATPase protein). The $K_{m,app}[NH_4^+]$ and V_{max} for the assays in the presence of increasing SCH28080 concentrations (125, 250, and 500 nM) were then determined.

Inhibition of the expressed wt H,K-ATPase is competitive as shown by the stepwise increase of the $K_{m,app}[NH_4^+]$ with

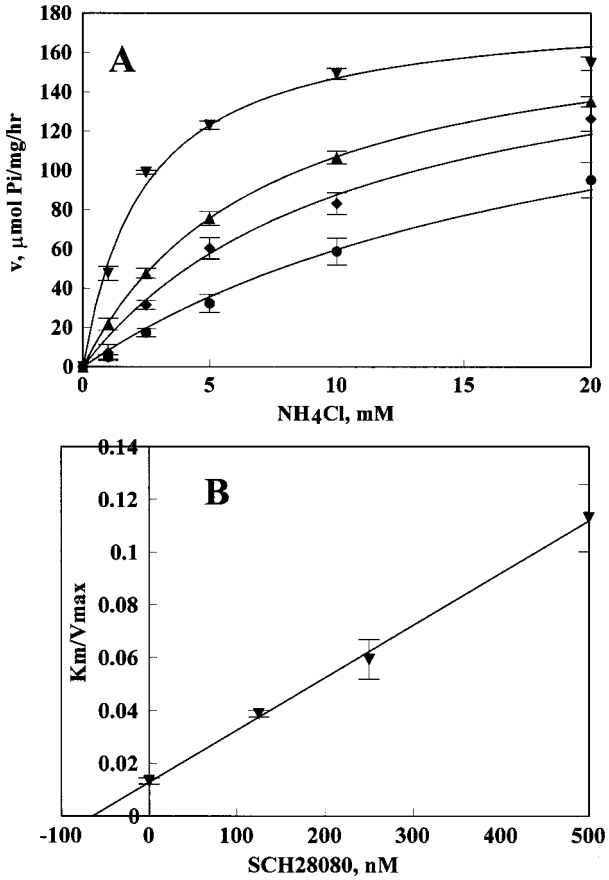

FIGURE 1: NH_4^+-stimulated ATPase activity of wild-type HK-ATPase. (A) Michaelis−Menten plot under different conditions: (▼) no SCH28080 (V_{max} = 182 ± 3.2 μmol mg^{-1} h^{-1}, K_m = 2.4 ± 0.2 mM); (▲) 125 nM SCH28080 (V_{max} = 183 ± 0.9 μmol mg^{-1} h^{-1}, K_m = 7.1 ± 0.2 mM); (◆) 250 nM SCH28080 (V_{max} = 182 ± 1.2 μmol mg^{-1} h^{-1}, K_m = 10.8 ± 1.3 mM); (●) 500 nM SCH28080 (V_{max} = 184 ± 1.3 μmol mg^{-1} h^{-1}, K_m = 20.8 ± 2.2 mM). (B) K_m/V_{max} replot. The points are K_m/V_{max} (the slopes of the inverse plot) vs SCH28080 concentration. The intersection with the *x*-axis of the linear regression of these points shows the negative K_i.

an unchanged V_{max}. The K_i, determined graphically by plotting $K_{m,app}/V_{max}$ for each inhibitor concentration against the corresponding SCH28080 concentration (Figure 1B), was 64 ± 11 nM SCH28080 for the wt enzyme. Hence, the expressed wt H,K-ATPase had the same kinetic characteristics as the hog gastric enzyme (G1 vesicles) (*28*−*30*).

Table 2 summarizes the results of the kinetic data for the mutants of the H,K-ATPase. Six mutations resulted in the complete loss of ion-stimulated activity, namely, Glu820Gln, Glu820Ala, and Glu343Ala and Glu343Asp, Glu936Val, and Lys791Ala. All other mutant enzymes retained ion stimulation and/or SCH28080 inhibition but with reduced V_{max}. The $K_{m,app}[NH_4^+]$ was not significantly changed for the mutants Glu820Asp, Asp824Glu, and Glu936Gln. Mutants Glu795Gln, Asp824Ala, and Asp824Asn displayed a lower $K_{m,app}[NH_4^+]$ (0.5−0.6 mM). In contrast, the $K_{m,app}[NH_4^+]$ was increased 3−4-fold for Glu795Asp and for Glu343Gln (8.1 ± 2.6 and 9.3 ± 0.8 mM), and about 2-fold for Glu936Asp and Lys791Ser (4.6 ± 0.2 and 4.7 ± 0.25 mM) (Table 2).

As shown in the kinetic analysis in the Appendix, the ratio V_{max}/K_m is proportional to the ratio of the dephosphorylation rate constant, *c*, and the intrinsic dissociation constant for NH_4^+ ions. This ratio provides a means of analyzing effects of NH_4^+. Although in some of the mutations the value of

Table 2: Expression Level and Kinetic Parameters of Wild-Type and Mutant H,K-ATPase

mutant	H,K-ATPase/ tot protein, %	$V_{max} \pm$ SE, μmol mg^{-1} h^{-1} [a]	$K_{m,app}[NH_4^+] \pm$ SE, mM	$V_{max}/K_{m,app}$-$[NH_4^+] \pm$ SE	H-ATPase act. $\pm$ SEM, μmol mg^{-1} h^{-1} [a]	K_i[SCH28080] $\pm$ SE, nM
E343A	7.7	0			0.33 $\pm$ 0.023	
E343D	7.8	0			0.16 $\pm$ 0.049	
E343Q	7.7	14.3 $\pm$ 0.5	9.3 $\pm$ 0.8	1.5 $\pm$ 0.2	0.34 $\pm$ 0.016	122 $\pm$ 24
E795Q	4.8	39.0 $\pm$ 1.1	0.6 $\pm$ 0.1	65.0 $\pm$ 12.7	0.96 $\pm$ 0.074	86 $\pm$ 31
E795D	4.5	9.6 $\pm$ 1.9	8.1 $\pm$ 2.6	1.2 $\pm$ 0.6	0.12 $\pm$ 0.051	700 $\pm$ 110
E820A	1.5	0			n/d[b]	
E820D	1.7	49.0 $\pm$ 1.0	2.3 $\pm$ 0.2	21.3 $\pm$ 2.3	0.60 $\pm$ 0.072	174 $\pm$ 63
E820Q	5.2	0			1.33 $\pm$ 0.050	
D824A	6.7	4.2 $\pm$ 0.4	0.5 $\pm$ 0.2	8.4 $\pm$ 4.2	0.40 $\pm$ 0.031	50 $\pm$ 22
D824N	4.0	1.6 $\pm$ 0.3	0.5 $\pm$ 0.6	3.2 $\pm$ 4.4	0.19 $\pm$ 0.025	n/d
D824E	1.8	12.0 $\pm$ 0.8	2.0 $\pm$ 0.3	6.0 $\pm$ 1.3	1.15 $\pm$ 0.063	162 $\pm$ 26
E936Q	0.6	40.0 $\pm$ 1.1	1.9 $\pm$ 0.6	21.1 $\pm$ 7.2	1.21 $\pm$ 0.18	84 $\pm$ 21
E936D	1.1	70.3 $\pm$ 1.0	4.6 $\pm$ 0.2	15.3 $\pm$ 0.9	0.72 $\pm$ 0.15	153 $\pm$ 24
E936V	2.6	0			n/d	
K791A	3.2	0			0.07 $\pm$ 0.042	
K791S	3.8	6.7 $\pm$ 0.14	4.7 $\pm$ 0.25	1.4 $\pm$ 0.1	0.21 $\pm$ 0.077	1325 $\pm$ 181
wt	2.1	182.0 $\pm$ 3.2	2.4 $\pm$ 0.2	75.8 $\pm$ 7.6	0.41 $\pm$ 0.059	64 $\pm$ 11

[a] Calculated per milligram of H,K-ATPase. [b] n/d: not determined.

$K_{m,app}[NH_4^+]$ was higher and in others the $K_{m,app}[NH_4^+]$ was lower than for wild type, for all mutants but one, the calculated ratio $V_{max}/K_{m,app}[NH_4^+]$ was significantly lower than for wild type. Three mutants, Glu820Asp, Glu936Gln, and Glu936Asp, displayed 3−5-fold lower values, and all the others from 9- to 64-fold lower values. Only one mutant, Glu795Gln, displayed a value of $V_{max}/K_{m,app}[NH_4^+]$ close to that of the wt enzyme (65.0 and 75.8, respectively).

The NH_4^+-independent H,K-ATPase (H-ATPase) activity is also informative regarding the effects of mutations. H-ATPase at 2.5 μM ATP was determined as the difference in P_i release in the absence and in the presence of 10 μM SCH28080. This low concentration of ATP sufficed to saturate this activity (not shown) and has the advantage of reducing SCH28080-insensitive ATP hydrolysis by the HEK293 cell membranes. In these conditions, SCH28080-insensitive P_i release varied from 0.06 to 0.11 μmol of P_i per total membrane protein in the membranes isolated from nontransfected cells, wt, and different mutants. In all cases, SCH28080 inhibited a significant fraction of the total P_i release. The H-ATPase specific activity was similar to the wt in Glu343Ala, Glu343Gln, and Asp824Ala, reduced about 2-fold in Glu343Asp, Asp824Asn, and Lys791Ser, and reduced about 4−5-fold in Glu795Asp and Lys791Ala. The H-ATPase activity was increased in Glu795Gln, Glu820Asp, Glu820Gln, Asp824Glu, Glu936Gln, and Glu936Asp compared to the wt. Previously, an increased K-independent pump-mediated ATPase activity has been reported for the Glu820Gln mutant (*31*). The results of Table 1 show that this phenomenon is not restricted to Glu820.

All the mutants examined, except Glu936Asp, retained competitive kinetics of inhibition by SCH28080. As a typical example of the competitive character of SCH28080 inhibition, data for the Asp824Glu mutant are presented in Figure 2A. The stepwise increase of the $K_{m,app}[NH_4^+]$ in the presence of increasing SCH28080 concentrations with V_{max} constant shows that SCH28080 inhibition remains strictly competitive also for this mutant. In contrast, the inhibition of Glu936Asp mutant H,K-ATPase by SCH28080 was noncompetitive as seen from the stepwise decrease of $V_{max,app}$ in the presence of increasing SCH28080 concentrations with $K_{m,app}[NH_4^+]$ constant (Figure 2B).

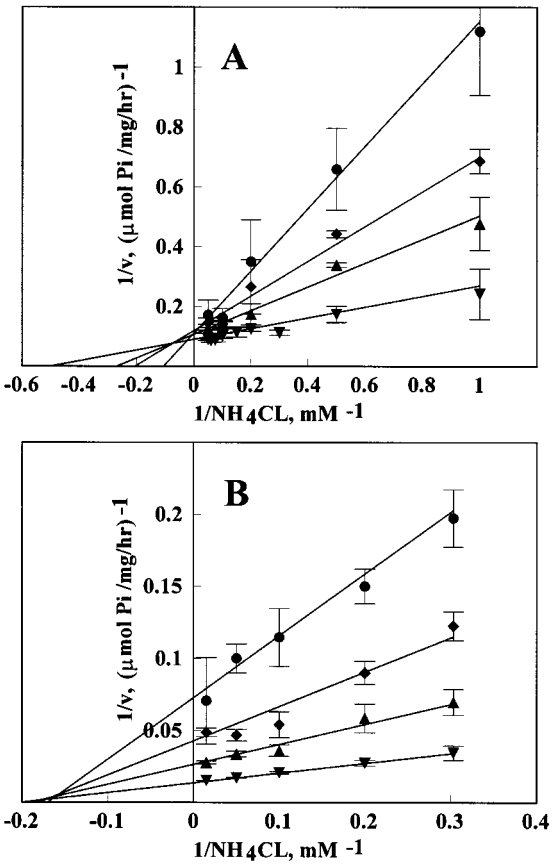

FIGURE 2: Inhibition of Asp824Glu (A) and Glu936Asp (B) mutant H,K-ATPases by SCH28080. Shown is the inverse plot of $1/v$ vs $1/[NH_4Cl]$: (▼) no SCH28080; (▲) 250 nM SCH28080; (◆) 500 nM SCH28080; (●) l−1000 nM SCH28080.

The most striking finding regarding inhibition by SCH28080 is the large increase in K_i[SCH28080] for the Lys791Ser and Glu795Asp mutants where the K_i increased to 1325 $\pm$ 181 and 700 $\pm$ 110 nM, respectively (Table 2, Figure 3). The mutations Glu936Asp, Asp824Glu, Glu343Gln, and Glu820Asp increased the K_i[SCH28080] 2−3-fold to 153, 162, 122, and 174 nM. The mutations Asp824Glu and Glu795Gln did not change the K_i[SCH28080], namely, 50 $\pm$ 22 and 86 $\pm$ 31 nM (Table 2).

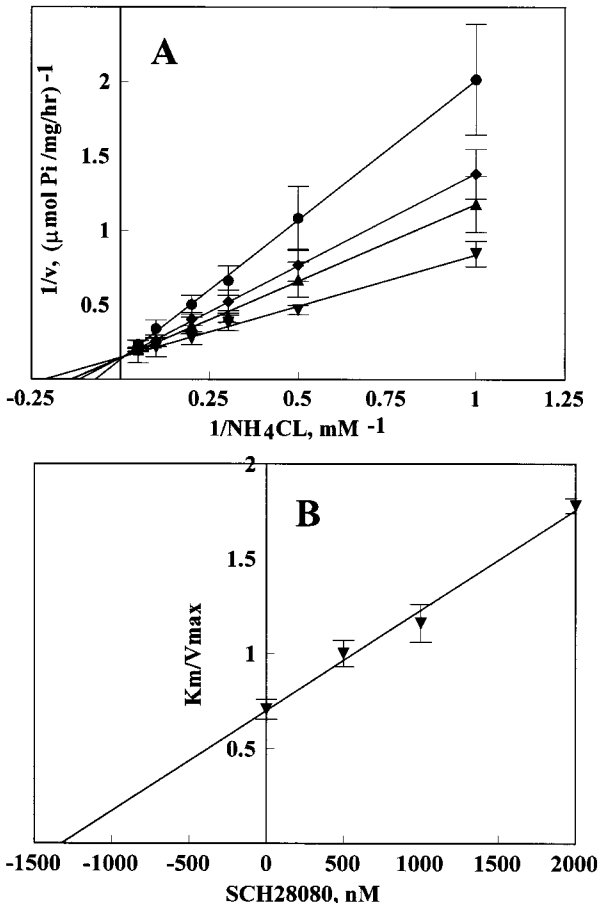

FIGURE 3: Inhibition of Lys791Ser by SCH28080. (A) The inverse plot of $1/v$ vs $1/[NH_4Cl]$: (▼) no SCH28080; (▲) 500 nM SCH28080; (◆) 1000 nM SCH28080; (●) 2000 nM SCH28080. (B) K_m/V_{max} replot. The points are K_m/V_{max} (the slopes of the inverse plot) vs SCH28080 concentration. The intersection with the *x*-axis of the linear regression of these points shows the negative K_i.

DISCUSSION

We recently reported the successful two-step transfection of HEK293, resulting in cell lines stably coexpressing the H,K-ATPase β subunit and wt or mutant H,K-ATPase α subunits (*7, 9*). The level of expression was sufficiently high to allow kinetic analysis in a variety of mutants. The limiting factor for successful kinetic analysis is the ratio between signal (ion-stimulated activity) and background (basal ATPase activity of the membranes from HEK293 cells in the absence of NH_4^+). When the signal over background was less than 8%, it was not possible to measure reliable kinetic parameters for SCH28080 inhibition. Modification of the procedure of growing the cells (as overgrown multilayers) and isolation of membranes resulted in a much higher content of H,K-ATPase in the membrane fraction [up to 8% as compared with 0.2−0.8% reported in our recent paper (*7*)]. This gives a 350% signal over background instead of the 64% reported earlier by us for the wt H,K-ATPase (*7*). The highest level of expression of H,K-ATPase achieved in the present study at 7.8% of total crude membrane protein is severalfold higher than in previous publications (*8, 19, 32*−*34*). This allows, for the first time, a detailed kinetic analysis of inhibitor affinity (K_i) and interactions of NH_4^+ with the expressed wt and mutant H,K-ATPase, even with mutants of low specific activity.

Previously, the role of specific amino acids in the membrane domain of P_2-type ATPases was defined largely by site-directed mutagenesis. The carboxylic and oxygen-containing amino acid residues in TM4−6 and TM8 in the sr Ca-ATPase and in Na,K-ATPase, homologous to the residues that were mutated in the present study, have been shown to be essential for ion binding and ATPase function (*10*−*16, 18*), consistent with the crystal structure of the calcium pump in the calcium (E_1) form at 2.6 Å resolution (*17*). Mutagenesis data on Glu343, Glu795, and Glu820 (*19, 33*−*36*) in H,K-ATPase had suggested a similar role of these three carboxylic residues in ion binding. The role of two other carboxylic acids, Asp824 and Glu936, as well as Lys791 in H,K-ATPase, has not been studied before. The results presented here (Table 2) show that most of the mutations resulted in large reductions in ATPase activity. Five of them caused a complete loss of ATPase activity, six reduced V_{max} by more than 10 times, and only four mutants retained more than 20% of wt activity.

The effects of the mutations on interactions with the NH_4^+ ion were analyzed by estimating the ratio $V_{max}/K_{m,app}[NH_4^+]$, which is proportional to c/K_d, the ratio of the dephosphorylation rate constant and dissociation constant for NH_4^+, as described in the Appendix. The use of the V_{max}/K_m ratio to analyze steady-state kinetic data allows conclusions about intrinsic binding constants of the ion, which cannot be made by inspection of K_m values alone.

The large reduction in the V_{max}/K_m observed for most mutants compared to wt could be due to a reduction in "*c*" or a rise in K_d or a change in both parameters. The large reduction in V_{max} itself of the different mutants is likely to have been caused by decreases in rate constants other than "*c*", since "*c*" is far from a rate-limiting step in the wild-type enzyme (*37*). The observation that the rate of NH_4^+-independent ATPase, which is a measure of "*c*" in the absence of NH_4^+, was reduced only moderately or even raised by the mutations shows that the intrinsic susceptibility to hydrolysis of the phospho−anhydride bond in Asp369 is not impaired. Thus, if the mutations caused any reduction in "*c*" in the presence of NH_4^+, it must be attributed to a reduced ability of NH_4^+ ions to accelerate dephosphorylation. Overall, the significantly reduced values of $V_{max}/K_{m,app}[NH_4^+]$ in most of the mutants indicate that in general the mutations increased the intrinsic NH_4^+ ion binding constant or reduced the ability of NH_4^+ ions to activate dephosphorylation; that is, these mutations alter the interaction of the protein with NH_4^+ ions. Hence, the results presented in Table 2 show that Glu343, Glu795, Glu820, Asp824, Glu936, and Lys791 are all important for NH_4^+ interactions with the protein.

This conclusion fits well with the mutagenesis results for other P_2-type pumps (*10*−*16, 18*). In the one case in which the V_{max}/K_m ratio was not markedly reduced, Glu795Gln, the simplest explanation would be that neither "*c*" nor K_d was strongly affected, implying that the charge on Glu795 is not important for NH_4^+ binding. Since the mutant Glu795Asp showed a large decrease in the V_{max}/K_m ratio, presumably here it is the length of the side chain that affects interaction with NH_4^+. A lack of effect of charge on ion binding affinity raises the question whether Glu795 is a direct contact residue.

The strictly competitive character of SCH28080 inhibition with respect to counterion (K^+ or NH_4^+) suggested that at least some of the residues involved in ion binding might

contribute also to the inhibitor binding. Accordingly, the mutations found to affect NH_4^+ interactions in H,K-ATPase were tested for their effect on SCH28080 affinity. Even though some of the mutants displayed less that 10% of wt activity and changed the K_m values for NH_4^+, K_i[SCH28080] defined kinetically allows the determination of the inhibitor dissociation constant. As long as mutant enzyme retains ion-stimulated activity, K_i[SCH28080] depends only on the rates of dissociation and formation of the dead end enzyme−inhibitor complex, and therefore reflects the true inhibitor dissociation constant. As seen from Table 2 and Figures 2 and 3, only three mutants were found to significantly affect SCH28080 inhibition; Glu795Asp and Lys791Ser greatly reduced the inhibitor affinity, while Glu936Asp changed the type of inhibition. The K_i[SCH28080] of Glu795Asp increased 11.5-fold compared to the wt. By contrast, the K_i-[SCH28080] for Glu795Gln was similar to the wt enzyme. Thus, the results suggest that the negative charge of Glu795 is not essential and that probably it is the length rather than the charge of the glutamate side chain that is important for SCH28080 interaction in this region. This is the same feature seen for the NH_4^+ interaction.

Two other mutants, Glu936Asp and Lys791Ser, displayed more dramatic changes in SCH28080 inhibition, and, interestingly, neither residue is conserved between the H,K-ATPase and the Na,K-ATPase. The substitution of Glu936 with the Val present in Na,K-ATPase led to a complete loss of ion-stimulated activity, and the mutation of Glu936 to Gln (22 wt % V_{max}) did not affect either inhibitor affinity or the nature of the kinetics (Table 2). The mutation Glu936Asp had 38% of the wt V_{max} and only slightly lower inhibitor affinity (increasing K_i[SCH28080] 2.4-fold) but changed the mechanism of inhibition from purely competitive to non-competitive (Figure 2B). It appears that the Glu936Asp mutation has changed the structure of the enzyme in this region to allow simultaneous binding of the cation and the protonated imidazopyridine. Thus, the negative charge of Glu936 is not essential for inhibitor binding, but the size of the side chain at position 936 determines exclusive binding of cation and inhibitor. The loss of competition between the ion and inhibitor in Glu936Asp with only slightly decreased ion and inhibitor affinity allows us to suggest that the binding sites of the ion and SCH28080 are mostly formed by different sets of amino acid residues. Together with the fact that the residues Glu343, Glu820, and Asp824 do not seem to affect inhibitor binding but are important for recognition of K^+ (or NH_4^+), inhibition of H,K-ATPase activity by SCH28080 could be a result of steric interference with ion binding rather than direct displacement of the cation.

The affinity for SCH28080 in the Lys791Ser mutant dropped by more than 20-fold. This is the largest effect on SCH28080 affinity that has ever been observed in mutagenesis studies of H,K-ATPase. Since the presence of this positively charged residue in the ion binding region is unique to the gastric H,K-ATPase as compared to the Na,K- or Ca-ATPase where serine substitutes for lysine, this suggests an important role of this residue in the SCH28080 selectivity of the H,K-ATPase versus other P_2-type ATPases. Mutation of Ser775 to Cys and Ala in the Na,K-ATPase resulted in a large decrease in K^+ affinity (13- and 31-fold) while Na^+ affinity was not much affected (*18*, *38*), so a role for Ser775 in ion binding and selectivity was postulated (*18*).

A model of the H,K-ATPase membrane region was constructed from the known 3D structure of the E_1 form of the sr Ca-ATPase with the aim of visualizing inhibitor binding (Figure 4). Homology within key structural regions among the P-type ATPases implies a conserved mechanism of ion transport and conserved placement of the ion sites within the membrane domain. This homology is confirmed by the present mutation results and visualized directly in the model.

However, a residue in the H,K-ATPase not present in any other pump is the positively charged Lys791 directly apposed to several of the carboxylate side chains of the ion site in this model. The first side chain dihedral angle of lysine in an α helix can be either ∼180° or ∼−60° with about equal probability. Figure 4A shows the orientation of Lys791 (final dihedral angle of 173°) where energy minimization gives hydrogen bond contacts with Glu820, Asp824, and Asn792. The other orientation of Lys791 (first dihedral angle of −70°) resulted in hydrogen bonding to Thr823, the backbone carbonyl of Glu936 in TM8, and possibly Tyr787 (not shown). The effect of the Lys791Ser, Glu795Asp, and Glu936Asp mutations on SCH28080 inhibition may result from a change in hydrogen bonding or charge pairing of Lys791 with one or more of the carboxylic acid residues. Small changes in the relative positions of TM5 and TM8 due to mutations of Lys791, Glu795, and Glu936 in the middle of the membrane domain could significantly change the distances between TM5, -6, and -8 on the extracytoplasmic surface of the membrane and result in loss of inhibitor affinity or change in the inhibitor and ion access.

It is tempting to speculate that the interaction of the protonated amino group of Lys791 with one or more of the carboxylic acids of the ion binding region in the E_2 conformation may promote release of the hydronium ion by lowering the pK_a. The importance of negative charge at positions 343, 820, and 824 makes these carboxylic acid residues possible candidates for hydronium or counterion transport sites. The relatively high levels of ion-stimulated activity in the neutral Gln mutants at positions 795 and 936 suggest that these may remain protonated during acid transport and therefore are not the side chains whose lowered pK_a's allow transport of hydronium ion into strong acid. It is also tempting to speculate that the orientation of Lys791 presented in Figure 4A would correspond to the E_2 conformation required for high-affinity inhibitor binding. According to the model presented, Lys791 hydrogen-bonds with the carboxylates of residues 820 and 824. Since residue 820 in the Na,K-ATPase is an aspartate rather than a glutamate, perhaps it is this residue whose pK_a is altered by Lys791, allowing release of hydronium ion at acidic pH.

The view from the cytoplasm in Figure 4B shows all the residues that were mutated in the present study as well as others whose mutation is known to affect SCH28080 binding [e.g., Cys813 (*7*), Ile816, and Thr823 (*8*) in TM6 and Met334 and Val337 in TM4 (*9*)]. The side chains of Met334 and Val337 point in a direction inconsistent with a binding site which would include Cys813 and Ile816. The explanation may be motion resulting in a different orientation of TM4 in the E_2 conformation to allow these residues to be involved in SCH28080 inhibition. Loss of inhibitor affinity in the Lys791Ser and Glu795Asp mutants would then be due to an allosteric effect of the mutations on the structure of the

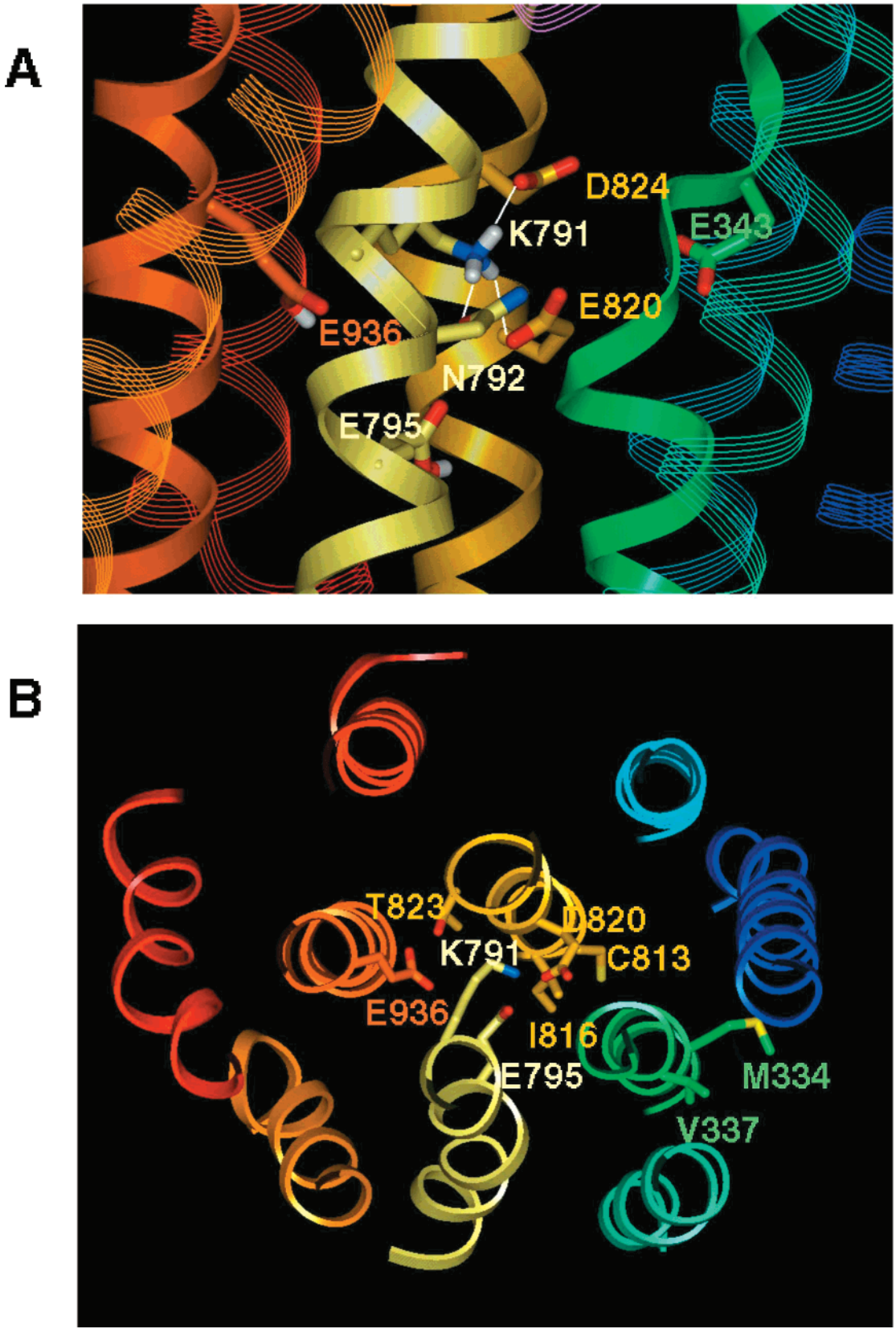

FIGURE 4: Energy-minimized homology model of the membrane domain of the H,K-ATPase built on the backbone coordinates of the sr Ca-ATPase. Only a few side chains in stick forms are shown for clarity. Membrane helices are colored according to the scheme of Toyoshima et al. (*17*) with TM1 dark blue, TM2 light blue, TM3 light green, TM4 dark green, TM5 light yellow, TM6 dark yellow, TM7 light orange, TM8 orange, TM9 dark orange, and TM10 red. (A) View from the membrane showing proposed hydrogen bonding between Lys791 (in one of two possible orientations) and Asp824, Glu820, and Asn792 in the ion binding pocket. Suggested charge states are indicated by the presence or absence of hydrogen on the terminal atoms of Lys791 and the carboxyl side chains. (In the alternative orientation, Lys791 would point between Glu936 and Thr823, leaving the site available for ion coordination.) (B) View of the membrane domain from the cytoplasm showing side chains where mutation has been shown to affect the apparent affinity for the specific imidazopyridine inhibitor SCH28080.

inhibitor binding site. Noncompetitive inhibition in the Glu936Asp mutant would be due to an effect on cation or inhibitor access, whereas the hydrophobic residues Ile816, Cys813, Met334, and Val337 would be implicated directly at the inhibitor binding site located one or two helix turns toward the extra-cytoplasmic face of the membrane domain from the ion binding site.

Photoaffinity labeling of the TM1/loop/TM2 region by a *p*-azidophenyl derivative of SCH28080 (*39*) places an additional restriction on the location of the inhibitor site. The para position of the phenyl ring at one end of the inhibitor structure must be next to a side chain from either TM1 or TM2. No site mutations affecting inhibitor binding have yet been identified in TM1 or TM2, and one or both of these helices may be at the periphery of the site.

In summary, the imidazopyridine moiety of SCH28080 in the protonated state appears to interact with a region of the protein near the luminal side and the negatively charged residues of the empty ion site in TM4, TM5, TM6, and TM8. The inhibitor binding site seems to be formed by residues different from ion binding residues, and inhibition of H,K-ATPase activity could be a result of steric interference with ion binding. The structure of the SCH28080 binding site depends on the presence of Lys791, Glu936, and Glu795 in H,K-ATPase. The hydrophobic phenyl ring interacts with TM1 or TM2. In this model of the H,K ATPase, several other amino acids are present in the region envisaged as responsible for SCH28080 inhibition, and mutations of these should further define the region for SCH28080 interaction.

ACKNOWLEDGMENT

Primary antibodies mAb 12.18 and 2B6 against the H,K-ATPase α and β subunits were generous gifts from Dr. A. Smolka and Dr. T. Masuda, respectively.

APPENDIX

A kinetic analysis of NH_4^+ activation of ATPase activity is based on the following scheme of the reaction mechanism:

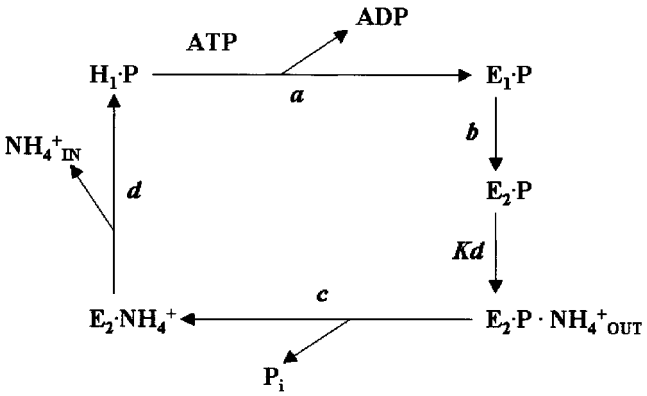

A simplifying assumption used in the derivations given below is that binding of one NH_4^+ ion suffices to activate the ATPase since the NH_4^+ activation curves are fitted by hyperbolic functions. A second assumption is that binding and dissociation of NH_4^+ ions are rapid enough so that binding is effectively in equilibrium. A third assumption is that all the steps in the cycle are unidirectional. This follows from the absence of products [ADP and P_i (steps a and c)] and insufficient H^+ or NH_4^+ concentrations to reverse steps b and d. With these assumptions, we can derive the following relationships, where E_t is the total enzyme concentration, *a*, *b*, *c*, and *d* are the rate constants for the different steps indicated in the scheme, and K_d is the dissociation constant for NH_4^+:

$$v = E_t abcd[NH_4^+]/(abc + abd + acd + bcd)/ \{[NH_4^+] + K_d abd/(abc + abd + acd + bcd)\} \quad \text{(A1)}$$

$$V_{max} = E_t abcd/(abc + abd + acd + bcd) \quad \text{(A2)}$$

$$K_m = K_d abd/(abc + abd + acd + bcd) \quad \text{(A3)}$$

After correction for the different expression levels, so that all E_t values are the same, the ratio of V_{max}/K_m for wild-type versus mutant enzymes is then given simply by $(c_{wt}/c_{mut})/(K_{d,wt}/K_{d,mut})$.

In the absence of NH_4^+, the dephosphorylation step, rate constant *c*, is by far the slowest step of the cycle. In this situation, $v = E_t c$. Thus, an independent measure of the relative values of *c* for wild-type and mutant enzymes, in the absence of NH_4^+, is given by the ratio of the rates of the NH_4^+-independent ATPase activity in the absence and presence of SCH28080.

REFERENCES

1. Goldshleger, R., Tal, D. M., and Karlish, S. J. (1995) *Biochemistry 34*, 8668−8679.
2. Shin, J. M., Kajimura, M., Arguello, J. M., Kaplan, J. H., and Sachs, G. (1994) *J. Biol. Chem. 269*, 22533−22537.
3. Sachs, G., Shin, J. M., Besancon, M., Munson, K., and Hersey, S. (1992) *Ann. N.Y. Acad. Sci. 671*, 204−216.
4. Besancon, M., Shin, J. M., Mercier, F., Munson, K., Miller, M., Hersey, S., and Sachs, G. (1993) *Biochemistry 32*, 2345−2355.
5. Shin, J. M., Besancon, M., Bamberg, K., and Sachs, G. (1997) *Ann. N.Y. Acad. Sci. 834*, 65−76.
6. Lutsenko, S., and Kaplan, J. H. (1992) *Ann. N.Y. Acad. Sci. 671*, 147−154; discussion 154−155.
7. Lambrecht, N., Munson, K., Vagin, O., and Sachs, G. (2000) *J. Biol. Chem. 275*, 4041−4048.
8. Asano, S., Matsuda, S., Hoshina, S., Sakamoto, S., and Takeguchi, N. (1999) *J. Biol. Chem. 274*, 6848−6854.
9. Munson, K. B., Lambrecht, N., and Sachs, G. (2000) *Biochemistry 39*, 2997−3004.
10. Clarke, D. M., Loo, T. W., Inesi, G., and MacLennan, D. H. (1989) *Nature 339*, 476−478.
11. Clarke, D. M., Loo, T. W., and MacLennan, D. H. (1990) *J. Biol. Chem. 265*, 6262−6267.
12. Nielsen, J. M., Pedersen, P. A., Karlish, S. J., and Jorgensen, P. L. (1998) *Biochemistry 37*, 1961−1968.
13. Kuntzweiler, T. A., Wallick, E. T., Johnson, C. L., and Lingrel, J. B. (1995) *J. Biol. Chem. 270*, 2993−3000.
14. Koster, J. C., Blanco, G., Mills, P. B., and Mercer, R. W. (1996) *J. Biol. Chem. 271*, 2413−2421.
15. Van Huysse, J. W., Kuntzweiler, T. A., and Lingrel, J. B. (1996) *FEBS Lett. 389*, 179−185.
16. Jewell-Motz, E. A., and Lingrel, J. B. (1993) *Biochemistry 32*, 13523−13530.
17. Toyoshima, C., Nakasako, M., Nomura, H., and Ogawa, H. (2000) *Nature 405*, 647−655.
18. Arguello, J. M., and Lingrel, J. B. (1995) *J. Biol. Chem. 270*, 22764−22771.
19. Asano, S., Matsuda, S., Tega, Y., Shimizu, K., Sakamoto, S., and Takeguchi, N. (1997) *J. Biol. Chem. 272*, 17668−17674.

20. Swarts, H. G., Hermsen, H. P., Koenderink, J. B., Willems, P. H., and de Pont, J. J. (1999) *Mol. Pharmacol. 55*, 541−547.
21. Stokes, D. L., Auer, M., Zhang, P., and Kuhlbrandt, W. (1999) *Curr. Biol. 9*, 672−679.
22. Bamberg, K., Mercier, F., Reuben, M. A., Kobayashi, Y., Munson, K. B., and Sachs, G. (1992) *Biochim. Biophys. Acta 1131*, 69−77.
23. Reuben, M. A., Lasater, L. S., and Sachs, G. (1990) *Proc. Natl. Acad. Sci. U.S.A. 87*, 6767−6771.
24. Lambrecht, N., Corbett, Z., Bayle, D., Karlish, S. J., and Sachs, G. (1998) *J. Biol. Chem. 273*, 13719−13728.
25. Bradford, M. M. (1976) *Anal. Biochem. 72*, 248−254.
26. Rabon, E. C., Im, W. B., and Sachs, G. (1988) *Methods Enzymol. 157*, 649−654.
27. Yoda, A., and Hokin, L. E. (1970) *Biochem. Biophys. Res. Commun. 40*, 880−886.
28. Wallmark, B., Briving, C., Fryklund, J., Munson, K., Jackson, R., Mendlein, J., Rabon, E., and Sachs, G. (1987) *J. Biol. Chem 262*, 2077−2084.
29. Faller, L. D., Rabon, E., and Sachs, G. (1983) *Biochemistry 22*, 4676−4685.
30. Rabon, E. C., and Reuben, M. A. (1990) *Annu. Rev. Physiol. 52*, 321−344.
31. Swarts, H. G., Hermsen, H. P., Koenderink, J. B., Schuurmans Stekhoven, F. M., and De Pont, J. J. (1998) *EMBO J. 17*, 3029−3035.
32. Rulli, S. J., Horiba, M. N., Skripnikova, E., and Rabon, E. C. (1999) *J. Biol. Chem. 274*, 15245−15250.
33. Swarts, H. G., Klaassen, C. H., de Boer, M., Fransen, J. A., and De Pont, J. J. (1996) *J. Biol. Chem. 271*, 29764−29772.
34. Asano, S., Tega, Y., Konishi, K., Fujioka, M., and Takeguchi, N. (1996) *J. Biol. Chem. 171*, 2740−2745.
35. Hermsen, H. P., Swarts, H. G., Koenderink, J. B., and De Pont, J. J. (1998) *Biochem. J. 331*, 465−472.
36. Hermsen, H. P., Koenderink, J. B., Swarts, H. G., and De Pont, J. J. (2000) *Biochemistry 39*, 1330−1337.
37. Brzezinski, P., Malmstrom, B. G., Lorentzon, P., and Wallmark, B. (1988) *Biochim. Biophys. Acta 942*, 215−219.
38. Blostein, R., Wilczynska, A., Karlish, S. J. D., Arguello, J. M., and Lingrel, J. B. (1997) *J. Biol. Chem. 272*, 24987−24993.
39. Munson, K. B., Gutierrez, C., Balaji, V. N., Ramnarayan, K., and Sachs, G. (1991) *J. Biol. Chem. 266*, 18976−18988.

BI0105328